Bioelectrochemistry 102 (2015) 1–9

Contents lists available at ScienceDirect

Bioelectrochemistry

journal homepage: www.elsevier.com/locate/bioelechem

A novel third generation uric acid biosensor using uricase electro-activated with ferrocene on a Nafion coated glassy carbon electrode

Tanushree Ghosh [a], Priyabrata Sarkar [a,*], Anthony P.F. Turner [b]

[a] Biosensor Laboratory, Department of Polymer Science and Technology, University of Calcutta, 92 A.P.C. Road, Kolkata 700 009, India
[b] Biosensors and Bioelectronics Centre, IFM, Linköping University, S-58183 Linköping, Sweden

ARTICLE INFO

Article history:
Received 26 May 2014
Received in revised form 5 November 2014
Accepted 8 November 2014
Available online 11 November 2014

Keywords:
Uricase
Ferrocene
Uric acid
Biosensor
Cyclic voltammetry
Differential pulse voltammetry

ABSTRACT

A new uric acid biosensor was constructed using ferrocene (Fc) induced electro-activated uricase (UOx) deposited within Nafion (Naf) on glassy carbon electrode (GCE). Electro-activation of UOx was successfully achieved by cyclic voltammetry through the electrostatic interaction of Fc with Trp residues within the hydrophobic pockets in UOx. The Naf/UOx/Fc composite was characterised by AFM, FTIR and EDX to ensure proper immobilisation. The interaction of Fc with the enzyme was analysed by Trp fluorescence spectroscopy and the α-helicity of the protein was measured by CD spectropolarimetry. The charge transfer resistance (R_{ct}), calculated from electrochemical impedance spectroscopy, for the modified sensor was lowered (1.39 kΩ) and the enzyme efficiency was enhanced by more than two fold as a result of Fc incorporation. Cyclic voltammetry, differential pulse voltammetry and amperometry all demonstrated the excellent response of the Naf/UOx/Fc/GCE biosensor to uric acid. The sensor system generated a linear response over a range of 500 nM to 600 μM UA, with a sensitivity and limit of detection of 1.78 μA μM^{-1} and 230 nM, respectively. The heterogeneous rate constant (k_s) for UA oxidation was much higher for Naf/UOx/Fc/GCE (1.0×10^{-4} cm s^{-1}) than for Naf/UOx/GCE (8.2×10^{-5} cm s^{-1}). Real samples, i.e. human blood, were tested for serum UA and the sensor yielded accurate results at a 95% confidence limit.

1. Introduction

Uric acid (UA) is the metabolic end product of purine and its derivatives in humans. A healthy human has 200–430 μmol/L UA in their blood. Excess serum UA results in deposition of urate microcrystals in joints, capillaries, skin and other tissues causing gout, hyperuricemia, Lesch–Nyhan syndrome, cardiovascular disease and Type-II diabetes. Lower UA levels also cause oxidative stress and multiple sclerosis in humans. Thus, detection of UA at various levels e.g. high, low and normal, is very important [1–3]. UA is conventionally determined by spectrophotometric and fluorimetric methods using the enzyme uricase [4,5]. Uricase (EC 1.7.3.3, urate:oxygen oxidoreductase enzyme; UOx) catalyses the oxidation of UA to allantoin in the purine degradation process. An alternative analytical approach that has emerged in recent years is the use of biosensors. UOx has proved advantageous for biosensor fabrication due to its selectivity and high specificity towards UA. Different biosensing systems have been described exploiting various modifications of electrodes for immobilisation of UOx on, for example, polyaniline [6,7], polypyrrole nanoelectrodes [8], ZnO nanorods [9], ZnO nano-flakes [10], CuO thin-film electrode surfaces [11] etc. Some researchers reported complex and costly modifications such as graphene/poly(acridine red)-modified electrodes [12], nanocrystalline graphite-like pyrolytic carbon films [13] and chemiluminescence biosensor chips using UOx-horseradish peroxidase (HRP), luminal [14] etc. However, UOx-based biosensors so far reported have not addressed adequately some aspects such as sensitivity, stability and linear range, repeatability and reproducibility. The main factors responsible for these limitations are degradation of the enzyme, poor signal transduction, low substrate affinity and deficiency of kinetically active enzymes after modification of the electrode surface. The most common approaches used in the transduction of the biochemical reaction to an electrical signal for enzyme-based amperometric biosensors are: (i) detection of redox active co-substrates or co-products such as oxygen and H_2O_2; and (ii) modification with electron mediators for electron exchange between the active site of the enzyme and the transducer. Biosensors based on the above two approaches exhibit some drawbacks as stated above [15] and at the same time suffer from leaching of soluble mediators from the electrode surface [16]. In third-generation biosensing systems, the electrons involved in the redox process are shuttled directly between the active site of the enzyme and the electrode surface to generate the response [17]. The main advantages of these systems are their potential to deliver interference free detection and high stability. However, the principal hurdle in developing direct electron transfer-based biosensors is the inaccessibility of the redox centre of most redox enzymes, which insulates electron flow between

* Corresponding author.

http://dx.doi.org/10.1016/j.bioelechem.2014.11.001
1567-5394/

the enzyme and the electrode. Among the various electron transfer mediators, ferrocene (Fc) and its derivatives have been widely used for developing biosensors. Conjugation of Fc with biomolecules such as DNA, amino acids and peptides can provide novel systems promoting electron transfer [18]. The inter-ring spacing of Fc is appropriate for hydrogen bonding and interaction through "π-stacking" with attached peptide strands [19]. The electrochemical behaviour of Fc ($Fc \rightarrow Fc^{+}$) attributed to the redox couple proved highly effective for electrode modification. Various Fc/glucose oxidase bioelectrodes have been developed to show the effectiveness of Fc derivatives in glucose sensors by cross-linking and by including ferrocene in the hydrophobic cavities of dextran polymers via host–guest reaction [20–24]. In Nafion (Naf) supported systems, Nafion was used as specific cation exchange membrane. Electrochemical deposition of cations within the micro-channels of Naf was achieved by Kumar and Sornambikai (2009) for sensor development [25]. In recent years, Naf/oxidase systems have been developed with different combinations of chemicals and electron mediators to enhance the sensitivity of sensors. Yumei et al. (2009) constructed a PyOD-FAD/β-CD/egg white/Fc-modified gold electrode for improved detection of pyruvate [26]. A Naf supported Fc-modified electrode was successfully used by Chen et al. (2011) in sensor development [27]. Zhao's group reported physical adsorption of UOx on to ZnO micro/nano-wires to prepare a Naf/UOx/ZnO/Au electrode for amperometric detection of UA [28]. A Au-MWCNT-Naf-AOx-PEI bioelectrode was fabricated by a simple drop casting method to prepare an ethanol biosensor and reported by Das and Goswami, in 2013 [29]. Another Naf/Fc modified oxidase was reported by Chinnadayyala et al. (2014) using a microwave technique for the development of 3rd-generation biosensors [17].

In the present study, the main focus has been to electrochemically entrap Fc into UOx in a cation selective polymer (Naf) platform to electroactivate the enzyme. Increase in catalytic efficiency of UOx was successfully achieved after electro-activation. Electrostatic retention of ferrocene was also supported by Trp fluorescence quenching study. The response behaviour and reaction kinetics were improved by the electro-activation procedure. The secondary structure of the enzyme after incorporation of Fc was investigated by circular dichoism (CD) spectroscopy. A detailed characterisation of electro-active UOx and a study of the stability of the bio-polymer composite were also undertaken. The electrochemical behaviour of the modified electrode was studied by cyclic voltammetry (CV) and electrochemical impedance spectroscopy (EIS). The response behaviour of the modified electrode with various UA concentrations was determined by differential pulse voltammetry (DPV) and amperometry. A linear range from 500 nM to 600 μM, with high selectivity, sensitivity and stability was obtained. Detection of uric acid in human serum samples was also successfully demonstrated using the modified bioelectrode.

2. Experimental

2.1. Reagents

Uricase (UOx; 80 U/mg) from *Comamonas* sp. BT UA (NCBI GenBank accession no. GU 265556 and microbial deposition no. NII1116, Microbial Culture Collection, National Institute for Interdisciplinary Science and Technology, Kerala, India) was extracted and purified in our laboratory at the University of Calcutta, India [30]. Nafion (Naf; 5 wt.%), ferrocene (Fc) and dopamine (DA) were purchased from Sigma-Aldrich, St. Louis, USA. Uric acid (UA), ascorbic acid (AA), xanthine (XA), urea (U), glucose (G) and L-cysteine were supplied by E Merck (Darmstadt, Germany). A 100 mM phosphate buffer saline (PBS) solution was used as electrolyte and was prepared from NaH_2PO_4, Na_2HPO_4 and NaCl procured from E Merck. All the reagent solutions and buffer solutions were prepared with Milli-Q water (18.2 MΩ). All experiments were conducted at room temperature (27 °C). Human blood serum samples were generously supplied by Dr's Trivedi and Roy diagnostic Laboratory, 93, Park Street, Kolkata-700016, India.

2.2. Preparation of Naf/UOx/Fc electrode

A glassy-carbon electrode (GCE) was polished with active alumina (0.05 μm) and washed first with ethanol 70% (v/v) and then Milli-Q water, three times in a sonication bath. UOx immobilisation was mediated by sequestrating the enzyme on the electrode surface along with a thin film of Nafion (Naf). Ferrocene (Fc) was incorporated into the Naf/UOx films by cyclic voltammetry (CV). In this modification process, an aqueous solution of UOx (5 μl from 1 mg/ml stock in 100 mM PBS; pH = 7.4) was mixed with 5 μl Naf solution (5 wt.% Naf in ethanol) and allowed to dry at room temperature. Fc incorporation was mediated by electrochemical conversion of Fc to Fc^{+} using potential scanning from 0 to 0.5 V, with a constant scan rate of 25 mVs^{-1} for 25 cycles against a Ag/AgCl reference (0.22 V, KCl saturated) electrode. Different Fc concentrations (1–10 mM bulk concentration) were used to minimise the charge transfer resistance of Naf/UOx/GCE. The electrode surface was then washed with distilled water to remove unbound Fc from Naf/UOx composite film. The retention capacity of the mediator within the film was monitored continuously for 25 cycles in a buffer. The structural stability and functional stability of UOx/Fc and Naf/UOx/Fc were studied in detail (methods and results are given in Supplementary materials 1; Figs. S1 & S2 are in the Supplementary materials 2).

3. Results and discussion

3.1. Electrochemical characterisation of Fc deposition

The electro-activation of UOx with Fc within the Naf/UOx composite was studied for 25 consecutive cycles of redox performance. Fc was electrochemically oxidised to ferrocenium (Fc^{+}) ion, which could move through the water channels to attach to the peptide strands of UOx on the electrode surface. In this process, the Fc^{+} molecules became reduced to Fc. The Fc molecules could not leak into the bulk solution because of the ion-selective membrane and, at the same time, could not remain in the water channels because of their hydrophobic nature. They (Fc) would preferably remain entrapped in the hydrophobic channels of the protein. Each successive redox cycle thus resulted in enhanced entrapment of Fc within the UOx matrix that could be calculated from the polarisation resistance. The redox nature of Fc was hindered for 1 mM and 10 mM bulk concentration (Fig. S3a & b) of Fc during deposition and resulted in distorted cyclic voltammograms. Well behaved redox behaviour was obtained for 5 mM Fc (bulk concentration) with increased peak current for consecutive cycles (Fig. S3c). The polarisation resistance (R_p) was calculated from the voltammograms for all the bulk concentrations of Fc and was found to be at its lowest (approx. 8499 Ω) for 5–8 mM Fc (Fig. S3d). The decreasing R_p value indicated the increasing ion transfer towards the working electrode. Incorporation of Fc within Naf/UOx may be higher with increasing bulk concentration of Fc [31]. The surface coverage, Γ of the electrode due to electro-deposition was evaluated using the following equation (Eq. (1)) and was found to be 1.86×10^{-5} mol cm^{-2}, where n is the number of electrons transferred per mole (during redox reaction), F is the Faraday constant, A is the surface area of electrode and Q is the charge under the anodic peak Fc oxidation [32].

$$\Gamma = Q/nFA \quad (1)$$

3.2. Characterisation of Naf/UOx/Fc composite by AFM, ATR-FTIR and EDX

The formation of a nano-porous matrix of Naf before and after UOx immobilisation was monitored by AFM. Very distinct differences in the surface structure were noted. A prominent regular porous structure

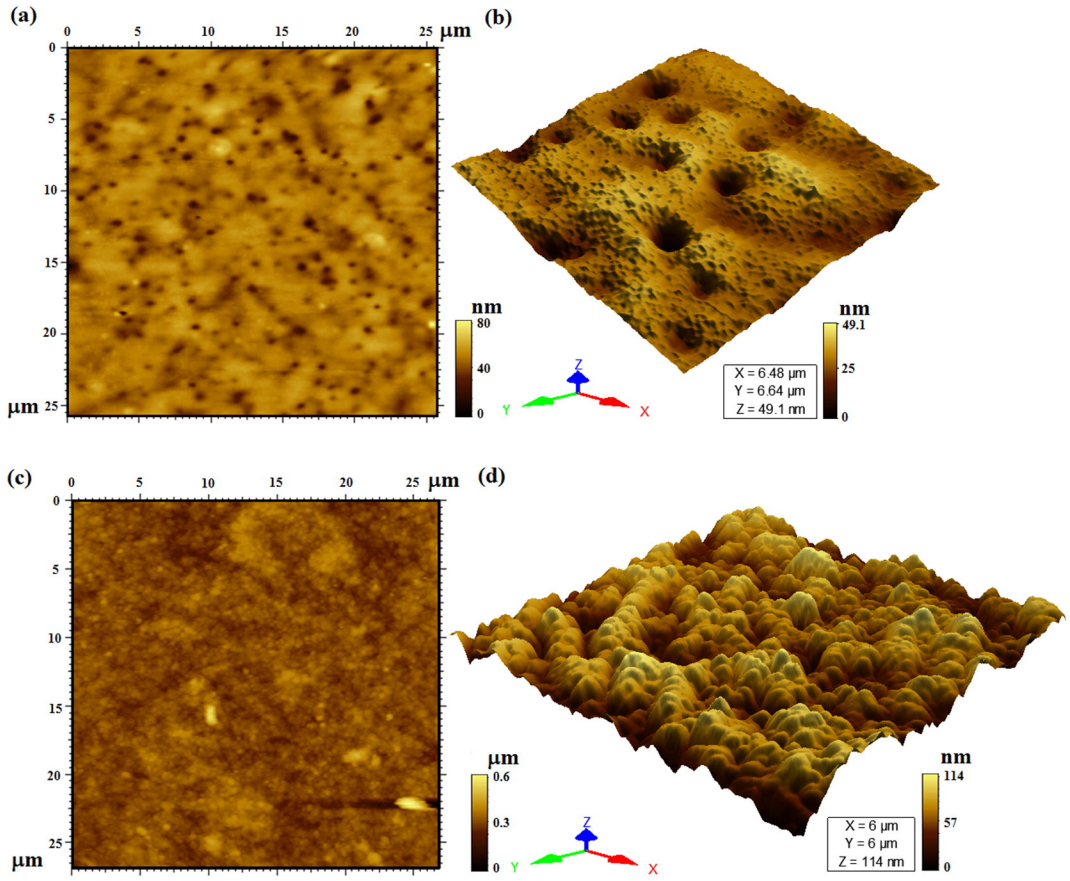

Fig. 1. AFM images obtained for Naf (a) and Naf/UOx composite (c). The magnified 3D images showed nanoporous surface for Naf film without UOx (b) and aggregated granular structures for Naf/UOx composite (d).

(Fig. 1a) was observed on Naf film without UOx, whereas UOx aggregation (Fig. 1c) around the porous matrix gave rise to a rather rough surface. When aqueous solution of UOx was mixed with Naf solution and allowed to dry at room temperature, it is possible that the acidic sulphonic groups self-organised into an array of water channels and UOx molecules aggregated in and around the channels. Fig. 1b shows a magnified 3D image (6.4 µm × 6.6 µm × 49 nm) of the nano-porous Naf film. The surface roughness and pore depth for Naf-modified electrodes were calculated from the extracted profile as 29 ± 4 nm and 15 ± 2 nm, respectively. Consequently, the surface roughness changed after UOx aggregation around the porous structures on the Naf film. Fig. 1d shows a magnified 3D image (6 µm × 6 µm × 114 nm) of UOx aggregated Naf composite. The surface roughness and pore depth were calculated as 89 ± 10 nm and 47 ± 4 nm, respectively. The huge change in surface roughness eventually confirmed the enzyme aggregation on Naf. Naf/UOx/Fc composite was further characterised by ATR-FTIR to compare with their signature peaks present in pure samples. FTIR of pure compounds (UOx, Naf and Fc) was compared with Naf/UOx and Naf/UOx/Fc composites (Fig. 2a). The bands observed at 1406 cm^{-1} were for asymmetric stretching vibration of C–C bonds of cyclopentadienyl rings of Fc. Bands at 1104, 999 and 813 cm^{-1} were assigned to the characteristic out-of-plane vibration of cyclopentadienyl rings [33]. The peak at 475 cm^{-1} could be due to asymmetric ring-metal stretching vibration of iron and cyclopentadienyl ring. Nafion gave rise to its characteristic peaks at 1146, 1054 and 981 cm^{-1}, which were due to symmetric stretching vibration of the sulphonic acid head group, C–O–C stretching vibration and C–F stretching vibrations, respectively. All the peaks were related to the sulphonated tetrafluoroethylene i.e. Nafion. UOx enzyme showed characteristic bands of polypeptide. Peaks at 3434 and 3339 cm^{-1} were for symmetric and anti-symmetric vibrations of N–H stretching, whereas the peaks at 1674 and 1595 cm^{-1} were for amide I and amide II vibrations of peptide bonds. EDX spectra of Naf/UOx (Fig. 2b; inset) and Naf/UOx/Fc (Fig. 2b) membranes showed characteristic features of successful modification. The inset spectrum of the Naf/UOx membrane showed characteristic peaks of carbon (25.32%), oxygen (6.92%), fluorine (59.31%) and sulphur (1.45%). The spectrum for the Fc-incorporated membrane confirmed the presence of iron with 32% atomic percentage along with an increase in the carbon peak (32.32%). These supporting data provided evidence of the incorporation of Fc within the modified membrane.

3.3. Electrochemical characterisation of modified electrode

The Nyquist and Bode plots (Fig. 3a,b and c) were obtained from EIS spectrum for bare GCE, Naf/GCE, Naf/UOx/GCE and Naf/UOx/Fc/GCE in 5 mM $K_3[Fe(CN)_6]$ containing 100 mM KCl solution at scanning frequencies from 0.001 Hz to 100,000 Hz, with a modulation amplitude of 0.01 V. Fig. 3a shows the Nyquist plots of GCE, Naf/GCE, Naf/UOx/GCE and Naf/UOx/Fc/GCE electrodes, where the real and imaginary parts of the impedance were calculated from the overall impedance. The obtained complex plane plots (Nyquist plots, $-Z''$ vs. Z') were fitted to equivalent circuit models using NOVA 1.9 (FRA compatible software). Two distinct semicircles were observed for all the spectra (Fig. 3a). The best fit with equivalent circuit model was $[R_s(R_{ct1} - CPE1)(R_{ct2} - CPE2)]$, similar to a partially polarisable electrode, where R_s referred to the solution resistance, CPE the constant phase element and R_{ct} the charge transfer resistance [34]. Here, the R_{ct1} and R_{ct2} were considered as the charge transfer resistances and CPE1 and CPE2 were pseudocapacitances of the electrode surface and the electrode–electrolyte interface of the corresponding semicircles,

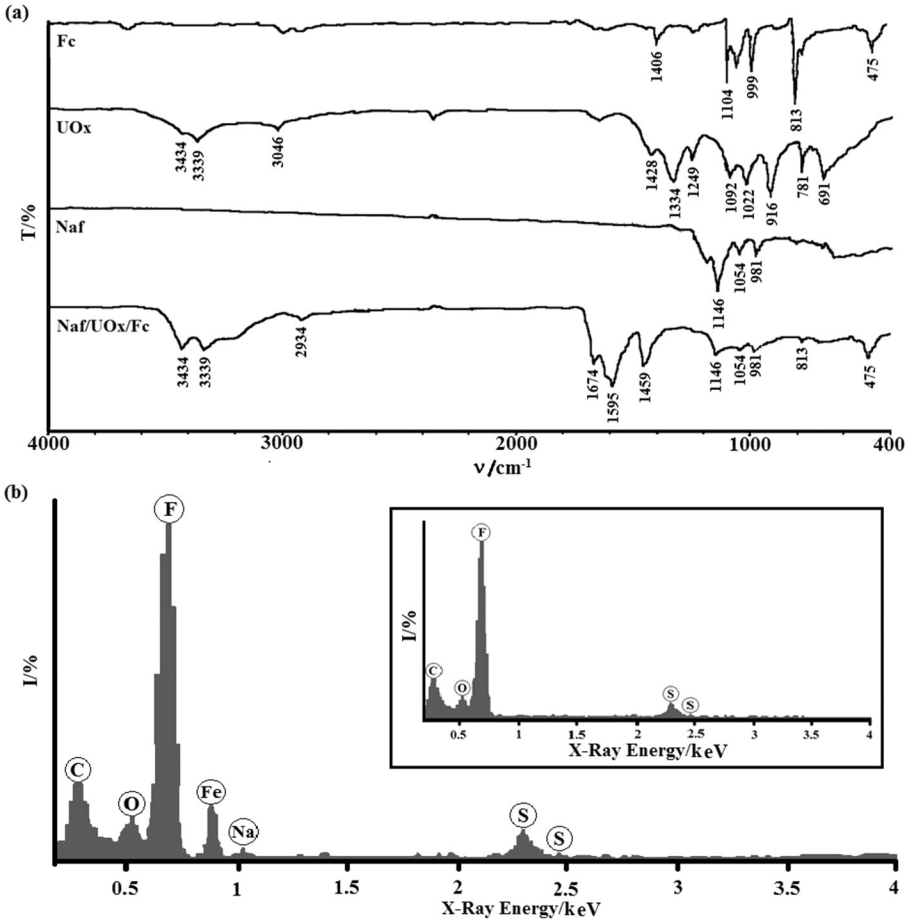

Fig. 2. ATR-FTIR and EDX spectra of Naf/UOx/Fc composite. FTIR spectra (a) obtained for pure Fc, UOx and Naf were compared with the spectra of Naf/UOx/Fc composite. EDX spectra (b) obtained for Naf/UOx/Fc composite were compared with Naf/UOx composite (b, inset).

respectively. The first semicircle was considered for its significant change in R_{ct} values (R_{ct1}) with different phases of electrode modification. The R_{ct} value of the Naf/GCE (8.69 kΩ; curve b) is much higher than the bare GCE (0.75 kΩ; curve a) suggesting the "blocking" of the electrode due to repulsion of the sulphonic acid head group of the Naf surface. Further immobilisation of UOx within Naf/GCE provided better conductivity, leading to significant reduction in the R_{ct} value (2.72 kΩ; curve c). Mixing of UOx with Naf provided a porous surface having hydrophilic channels surrounded by UOx aggregates (as shown in the surface morphology study using AFM). Electrodeposition of Fc facilitated charge transfer by reducing the R_{ct} value still further (1.39 kΩ; curve d), resulting in better electron transfer between the solution and the electrode surface.

Fig. 3b depicts the Bode amplitude plots (Log |Z| vs. Log f) and Fig. 3c shows the Bode phase angles for bare GCE, Naf/GCE, Naf/UOx/GCE and Naf/UOx/Fc/GCE. Bode phase diagrams contained two characteristic frequency peaks for bare GCE, Naf/GCE, Naf/UOx/GCE and Naf/UOx/Fc/GCE. In the frequency range from 10^5 to 10^4 Hz, the |Z| value was almost constant and the phase angles approached zero, indicating the same solution resistance (R_s) for all the modification stages of GCE. In the

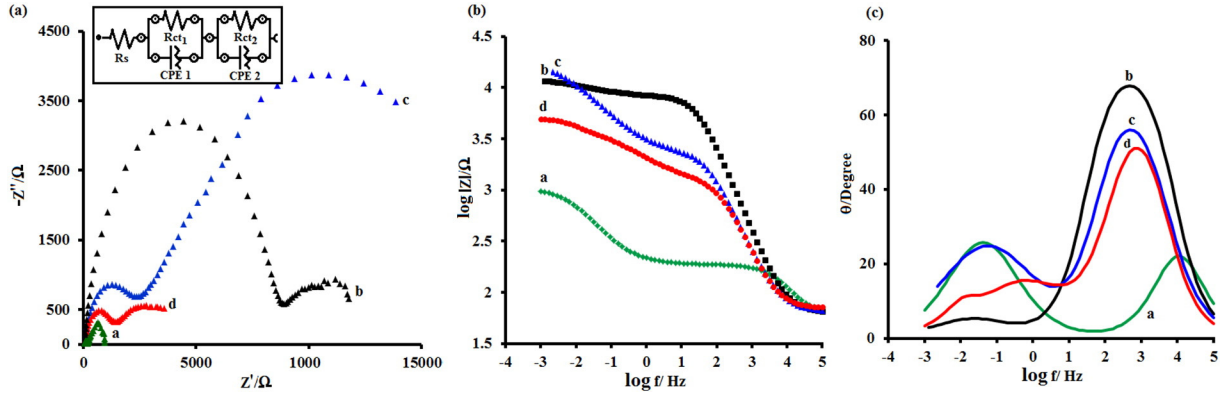

Fig. 3. Nyquist (a) and Bode (b and c) plots of bare and modified electrodes. The equivalent circuit model (a, inset) used for fitting the impedance spectra. The curves represented the results obtained for bare GCE (curve a), Naf/GCE (curve b), Naf/UOx/GCE (curve c) and Naf/UOx/Fc (curve d).

frequency range from 10^4 to 10^2 Hz, the |Z| value increased (curves b, c and d) and the phase angle reached a peak (between 10^3 to 10^2 Hz), indicating the growing role of a capacitive response with decreasing frequency. A 90° phase angle corresponds to an ideal capacitor, whereas phase angles of less than 90° indicate that the charge transfer reaction is facilitated due to pinholes or defective electrode coating [34]. The Naf/GCE showed a maximum phase angle of 67.89° (curve b) and moved towards an ideal capacitor, whereas the Naf/UOx and Naf/UOx/Fc electrodes showed lower phase angles such as 56.05° (curve c) and 51.08° (curve d). This indicated that the charge transfer was facilitated by the modified electrode. The |Z| values remained constant for bare GCE and Naf/GCE electrodes (R_{ct1}) in the frequency range from 10^2 to 10^0 Hz. The Naf/UOx, Naf/UOx/Fc-modified electrodes and bare GCE showed a second capacitive response at about 10^{-2} Hz. In the frequency range from 10^0 to 10^{-3} Hz, the |Z| values reached equilibrium. The |Z| values were 0.95 kΩ for bare GCE, 11.77 kΩ for Naf/GCE, 15.07 kΩ for Naf/UOx/GCE and 4.66 kΩ for Naf/UOx/Fc/GCE. This denotes that |Z| is equal to the total resistance ($R_s + R_{ct1} + R_{ct2}$) of the system (Table S1). Since the solution resistance was same for all, the R_{ct} value (R_{ct1}) decreased with electrode modification, and thus facilitated electron transfer.

3.4. Electrochemical kinetics of UA determination

The anodic peak potentials of UOx/Fc-modified electrodes were studied in the presence of 500 μM uric acid. The oxidation potential of UA was recorded at 0.342 V for 5 mM Fc bulk concentration. The response to UA was characterised for bare GCE, Naf/GCE, Naf/UOx/GCE and Naf/UOx/Fc/GCE electrodes (Fig. 4a). The voltammograms (Fig. 4a, curve: a & b) showed no redox peaks because of the unavailability of a redox couple and lack of sensitivity of Naf towards UA. In the Naf/UOx-modified system, one oxidation peak at 0.618 V was obtained for UA due to substrate specificity of the enzyme (Fig. 4a, curve: c). Electro-activated UOx showed a redox couple at 0.168 V/0.081 V (Fig. 4a, curve: d) in a buffer, indicating the successful incorporation of Fc within the protein matrix. For Naf/UOx/Fc, a negative shift of the peak potential for UA oxidation (about 276 mV) was observed (Fig. 4a, curve: e). The introduction of Fc significantly accelerated electron transfer from the catalytic site of UOx to the electrode surface. This is evidenced by the emergence of the highest peak current at a much lower potential [35,36]. This lowering of oxidation potential is likely to prove beneficial for the avoidance of interference due to the presence of other oxidisable species. The following equations (Eqs. (2), (3) and (4)) illustrate the possible reactions [37,38].

$$\mathrm{UOx/Fc} - e^- \rightarrow \mathrm{UOx/Fc^+} \quad \text{.....Electrochemical Oxidation} \tag{2}$$

$$\text{Uric acid} + \text{Oxygen} \xrightarrow{\mathrm{UOx/Fc+}} \text{Allantoin} + CO_2 + 2H^+ + 2e^- \quad \text{.....Enzymatic Oxidation} \tag{3}$$

$$\mathrm{UO/Fc^+} + e^- \rightarrow \mathrm{UOx/Fc} \quad \text{.....Electrochemical Reduction} \tag{4}$$

Oxidation of uric acid (UA) on Naf/UOx/Fc electrodes showed increasing peak current with decreasing H^+ concentration of reaction buffer, from pH = 5 to 7.4 (Fig. S4a). Further increase in pH gave rise to a sudden fall in oxidation peak current (pH = 8 to 10). The effect of pH on peak potentials was very interesting. Redox peak potentials of Fc (Ep_a and Ep_c) remained unchanged for all the pH conditions, whereas the oxidation peak potential for uric acid ($Ep_{a[UA]}$) changed in two steps. $Ep_{a[UA]}$ shifted to more positive potential with increasing pH (i.e. decreasing proton concentration) up to 7.4 and then decreased gradually. The slope of the anodic potential of $Ep_{a[UA]}$ versus pH was calculated as 36 mV/pH unit (pH = 5 to 7) and 41 mV/pH unit (pH = 7.4 to 10). We could thus conclude that the reaction potential was pH dependent and it might follow the Nernstian two-proton two-electron system, comparable to the enzymatic oxidation reaction of uric acid.

The electrochemical response of the Naf/UOx/Fc-modified electrodes was also characterised by CV by observing UA oxidation at progressively increasing scan rates from 10 to 100 mVs^{-1} (Fig. 4b). The three observable peak currents and peak potentials were analysed. The anodic and cathodic peak currents (*Ipa* and *Ipc*) for the Fc redox couple were linearly proportional to the square root of the scan rate (Fig. S4b). With increasing scan rate, an equivalent increase in cathodic peak current (*Ipc*) was observed without any shift in peak potentials (Ep_a and Ep_c). This is a characteristic of fast redox reactions having rapid electron transfer kinetics. The peak separation ($\Delta Ep = Ep_a - Ep_c$)

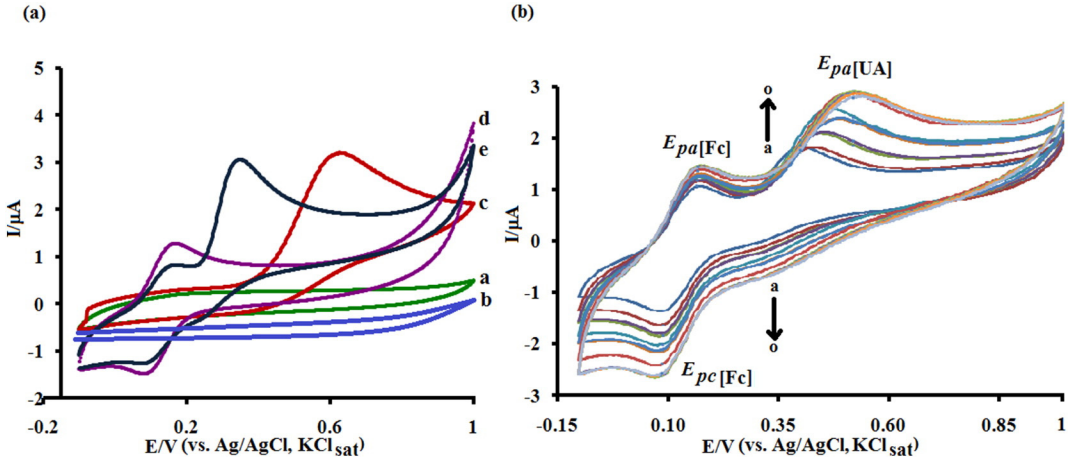

Fig. 4. CV obtained for bare and modified electrodes at different stages of modification (a). The bare (curve a) and Nafion coated GCE (curve b) gave no peak in buffer and UA, respectively. Naf/UOx/GCE (curve c) and Naf/UOx/Fc/GCE (curve e) gave prominent oxidation peaks in presence of UA with a negative shift of 276 mV in peak potential for Naf/UOx/Fc/GCE. The Naf/UOx/Fc/GCE (curve d) gave signature peak of Fc in buffer without UA. The reaction kinetics obtained by CV at scan rates from 10 to 100 mV s^{-1} (b; curve a–o). All the studies were conducted with 500 μM UA in 100 mM PBS (pH = 7.4).

of $Fc \leftrightarrow Fc^+$ was found to be 61 ± 4 mV, which corresponds to a single electron redox reaction. This was comparable to a reversible reaction showing Nernstian behaviour (ΔEp = 59 mV/n). The deviation in peak potential might be due to coupling of a comparatively slower irreversible reaction with this redox reaction. Coupling of a chemical reaction with the electrochemical redox reaction was also characterised by examining the peak current ratio. The ratio of reverse to forward peak current (i_{pr}/i_{pf}) increasingly deviated from unity (1.3 to 2) with increasing scan rate for the Fc redox reaction. This observation strongly suggests that the chemical reaction, i.e. enzymatic oxidation of UA, was coupled with the Fc-redox reaction. The oxidation of Fc donated one electron on the electrode surface. Simultaneous oxidation of UA gave rise to two protons and two electrons and the latter were readily accepted by Fc^+. The CV showed significant changes in the UA oxidation peak, which was very prominently related to the Fc^+ reduction peak. On the other hand, negligible changes in the Fc oxidation peak potential were observed. The oxidation peak potential ($Ep_{a[UA]}$) increased with increasing scan rate and a prominent shift in peak potential was observed. The total shift in peak potential reflected the irreversible reaction and the transfer coefficient "α" was calculated by wave log analysis of the individual oxidation peak of UA (for different scan rates). The peak potential ($Ep_{a[UA]}$) and half peak potential ($Ep_{/2}$) differ by 48/αn mV for irreversible and quasi-reversible systems [32].

$$Ep - Ep_{/2} = 48/\alpha n \quad (5)$$

From this relationship (Eq. (5)) the number of electrons involved in the charge transfer reaction was calculated as 2.2 ± 0.3 for different scan rates (10–100 mV s^{-1}). The diffusion coefficient was calculated to be 2.42×10^{-8} cm^2 s^{-1} from the following equation (Eq. (6)) at 25 mV s^{-1} scan rate and at the highest peak current for the oxidation of 500 μM uric acid [32].

$$i_p = \left(2.99 \times 10^5\right) n(\alpha n_a)^{1/2} C D^{1/2} v^{1/2} \quad (6)$$

where i_p is the current density (A cm^{-2}), n is the number of electrons involved in the charge transfer step, D is the diffusion coefficient (cm^2 s^{-1}), v is the scan rate (V s^{-1}) and C is the concentration (mol cm^{-3}).

The heterogeneous rate constant (k_s) value was calculated using the Velasco equation (Eq. (7)) for Naf/UOx/GCE and Naf/UOx/Fc/GCE to understand the facile electron transfer due to Fc deposition [39].

$$k_s = 1.11 D_o^{1/2} \left(Ep - Ep_{/2}\right)^{-1/2} v^{1/2} \quad (7)$$

where k_s is the standard heterogeneous rate constant, D_o is the apparent diffusion coefficient (cm^2 s^{-1}), Ep is the oxidation peak potential (V), $Ep_{/2}$ is the half-wave oxidation peak potential (V) and v stands for scan rate (V s^{-1}). The estimated k_s values for Naf/UOx- and Naf/UOx/Fc-modified electrodes were found to be 8.18×10^{-5} cm s^{-1} and 1.02×10^{-4} cm s^{-1}, respectively. The k_s value for UA oxidation on Fc-activated bioelectrode was faster than on the Naf/UOx electrode.

DPV for different concentration ranges of UA (Fig. 5a) was measured on Naf/UOx/Fc/GCE. DPV was run over a potential range from 0.2 to 0.6 V with a step potential of 0.01 V, modulation amplitude of 0.049 V and modulation time of 0.05 s. The UA oxidation peak (at 0.370 V) current was increased with each increment of 25 μM UA (Fig. 5a, curve a–j) in 100 mM PBS (pH = 7.4). The effect of UA on Naf/UOx/Fc/GCE was also characterised by EIS in 100 mM PBS (pH = 7.4). Fig. 5b shows the Nyquist plot with increased UA concentrations plotted with the complex plane of the modified electrode. In the presence of UA, the Warburg impedance (Z_w) seemed to be dominant and the best fit equivalent circuit [$R_s(R_{ct1} - CPE1)((R_{ct2} - CPE2)W)$] was obtained (Fig. 5b, inset). An increase in R_s and R_{ct1} values was observed (Fig. S5a) with higher UA concentrations. The Bode phase (Fig. S5b) and Bode modulus (Fig. S5c) plots were indicative of diffusion-limited behaviour. The phase shift towards 45° in the frequency range 10^1 Hz to 10^{-2} Hz confirmed the Warburg impedance.

3.5. Amperometric determination of UA

The UA standard curve (Fig. 6) was linear over the concentration ranges 500 nM to 50 μM, with a sensitivity of 1.78 μA/μM (slope of the standard equation Y = 1.78X + 0.13) and 25 μM to 600 μM, with a sensitivity of 1.86 μA/μM (slope of the standard equation Y = 1.86X + 12.3). The correlation coefficient was found to be 0.99 for both the concentration ranges. The limit of detection (LOD = 3 × SD) and limit of quantification (LOQ = 10 × SD) of UA were calculated as 230 nM and 770 nM (for lower range), respectively. The kinetics of Naf/UOx/Fc was calculated using the apparent Michaelis–Menten constant [K_m'']. The maximum current response i_{max} and K_m'' were calculated from the intercept and slope of the plot 1/current vs. 1/[S] (Fig. S6a). These values were evaluated as 35 nA μM^{-1} and 14.07 μM, respectively. The affinity of the enzyme towards the substrate was much higher (the lower the K_m'' value, the higher the substrate affinity) and this reflected its high sensitivity. The response time for UA was very fast e.g. 5 s. The UOx/Naf/Fc exhibited good stability registering 98% of the maximum response even after 50 days (Fig. S6b). A repeatability study was conducted under the same laboratory conditions for 24 measurements with 50 μM UA using different electrodes modified in the same manner. A reproducibility study was also

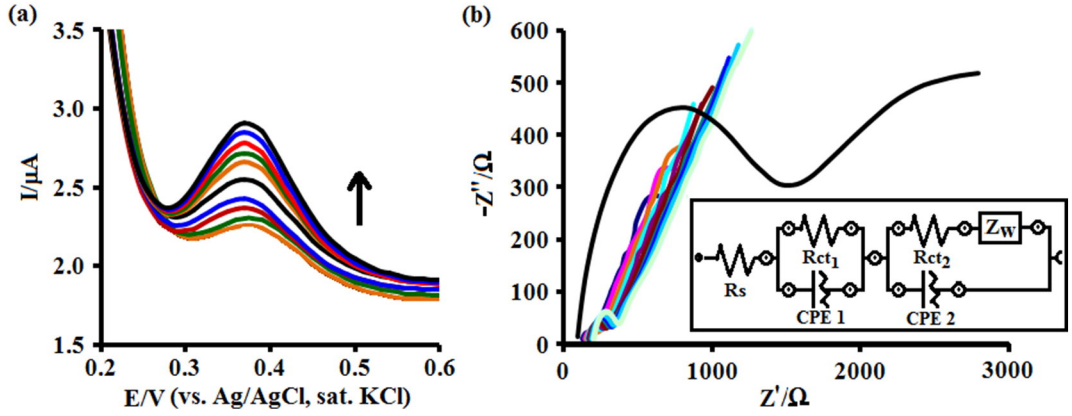

Fig. 5. DPV obtained for each increment of UA concentrations (curves from 25 μM to 250 μM with increment of 25 μM) in 100 mM PBS, pH = 7.4 (a). The Nyquist plot of Naf/UOx/Fc modified electrode in 5 mM $K_3[Fe(CN)_6]$ containing 0.1 M KCl (b) compared with the same in presence of increased concentration of UA.

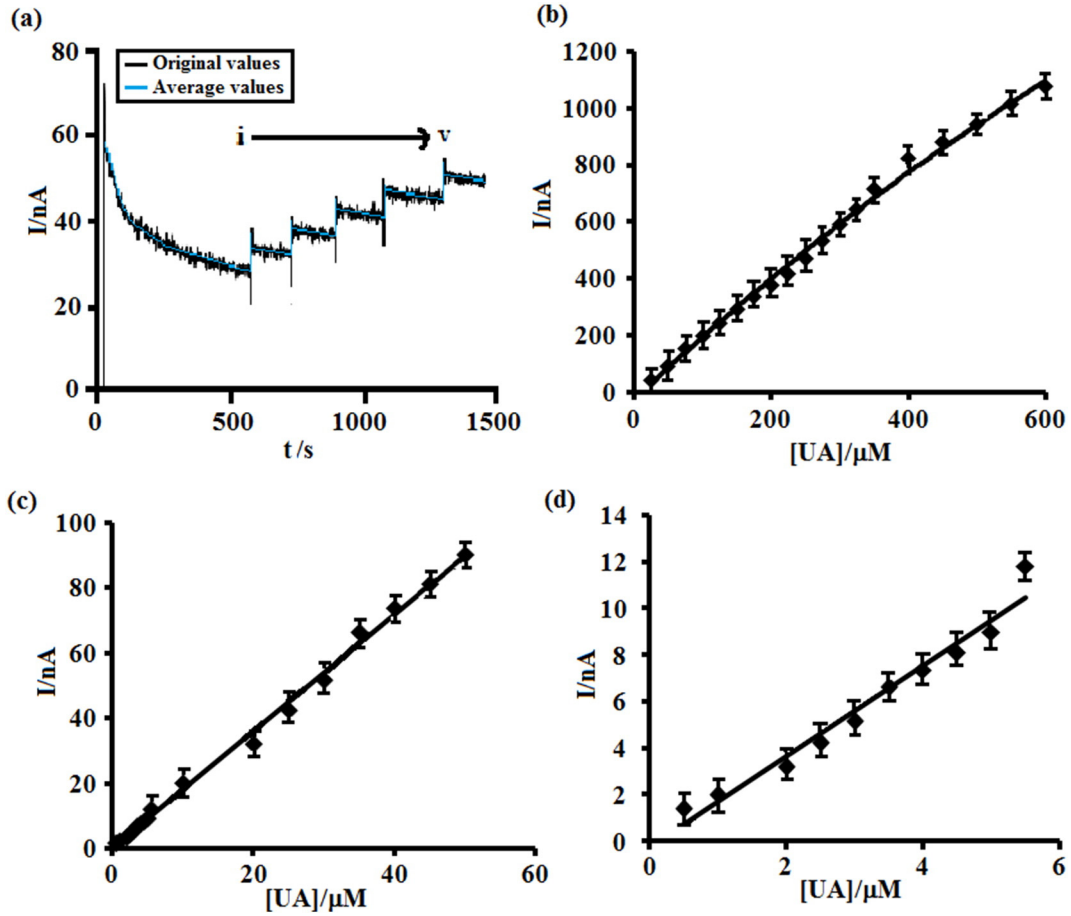

Fig. 6. Amperometric i–t curve for determination of UA with Naf/UOx/Fc/GCE in 100 mM PBS solution (pH = 7.4), applied potential 0.342 V (a) under homogeneous stirring. Each addition increases 25 μM of UA concentration. Calibration plot of UA at different concentration ranges (b, c and d). (b) [UA]/μM vs. I/nA for 25–600 μM of UA, I/nA = (1.86 ± 0.17) [UA]/μM + (12.39 ± 0.08)/nA, slope: (1.86 ± 0.17) nA μM^{-1}. (c) [UA]/μM vs. I/nA for 5–50 μM of UA, I/nA = (1.78 ± 0.11)[UA]/μM + (0.30 ± 0.009)/nA, slope: (1.78 ± 0.11) nA μM^{-1}.(d), [UA]/μM vs. I/nA for 0.5–5.5 μM of UA, I/nA = (1.77 ± 0.12) [UA]/μM + (0.119 ± 0.07)/nA, slope: (1.77 ± 0.12) nA μM^{-1}.

performed by making 24 measurements on different dates and under different environmental conditions (temperature, humidity) using an AUTOLAB PGSTAT 30 analyser). The precision of the results was analysed statistically using the h-test (repeatability) and k-test (reproducibility). The coefficients of variation were found to be only 1.6% and 2.1%, respectively.

3.6. Interference study and UA detection in human serum

An interference study was conducted using amperometry with potential constituents present in human serum such as ascorbic acid (AA), urea (Ur) and glucose (G). Additionally, the specificity of the UOx/Naf/Fc-modified electrode response was tested against xanthine (XA), given its structural similarity with uric acid (Fig. S7a). The potentially interfering species DA (1 mM), Ur (1 mM), AA (0.1 mM), Xn (1 mM), G (5 mM) and L-cysteine (1 mM) were used one at a time in the presence of a 500 μM of UA and the amperometric response at a fixed potential (0.342 V) was recorded as a function of time. The selectivity coefficients (K_{sel}), were determined for the same potential using the following relation (Eq. (8)) [40]

$$K_{sel} = [(\Delta I_t/\Delta I_i) - 1] \times Ci/Cj \quad (8)$$

where $\Delta I_t = I_t - I_b$ and $\Delta I_i = I_i - I_b$, I_t is the value of the current recorded for the mixed PBS having uric acid and interfering species. I_i is the value of current recorded for only uric acid (500 μM), I_b is the corresponding current recorded for the blank PBS (without analytes) and Ci and Cj are the concentrations of uric acid and interfering species, respectively in PBS solution. The values for the selectivity coefficient obtained for the various interfering agents are listed in Table-S2. Since the order of magnitude of these values was 10^{-3} or less, it was concluded that the tested species did not significantly interfere with the biosensor response to uric acid. Hence, the designed UOx/Naf/Fc/GCE biosensor is highly selective for the amperometric determination of uric acid. Five human serum samples (Fig. S7b) were tested with the Naf/UOx/Fc biosensor (Table-S3). A paired Student's t-test was performed five times (n = 5) for five different samples. The calculated values using the biosensor showed no significant difference from the results provided by our clinic (spectrophotometric method). It was found to be at the 95% confidence level with 8 degrees of freedom for all the five samples.

3.7. Comparison of biosensor performance

The performance of the proposed sensor was compared with that of other UA biosensors reported in literature and detailed in Table S4. It was observed (Table S4) that the present system produced the lowest K_m value and hence the sensor's affinity towards its substrate was the highest. The range of detection was observed to be wider than the other sensors. While our sensor registered sensitivity in μA μM^{-1}, others obtained sensitivities of μA mM^{-1}. The stability of the sensor was high with a much lower detection limit, as shown in the comparison table. A Table of comparison (Table S5) is also provided to address

the performance of the enzyme-based electro-active matrix and draw attention to the gain due to the electro-activation presented in this work. Table S5 shows different enzymes that were modified to achieve higher sensitivities together with their corresponding biosensors. Electrochemical activation of an enzyme by incorporation of a redox active species has not been reported earlier. The electro-active UOx in our system showed comparable substrate affinity with a high turnover (K_{cat}) number.

4. Conclusions

We have successfully demonstrated the electrochemical incorporation of Fc within a Naf/UOx composite. Characterisation of the modified composite using AFM, FTIR and EDX confirmed the proposed modification. The electro-activation of the UOx was confirmed by cyclic voltammetric studies. The small reduction in α-helicity of electro-active UOx, as confirmed by CD studies, suggests a spatial interaction of Fc with the UOx and also confirms the stability of the protein. The electro-activation of the enzyme enhanced its catalytic efficiency (K_{cat}/K_m) by more than two fold. We have also inferred insertion of the Fc molecules inside the hydrophobic region of the protein molecules from the observations made in a Trp fluorescence quenching study. The CV and EIS spectral analyses illustrated that the conductive behaviour of Naf/UOx/Fc/GCE was better than that of Naf/UOx/GCE. The electro-activated Naf/UOx/Fc/GCE proved to be an efficient transducer for UA detection (LOD = 230 nM) using both DPV and amperometry. Fc incorporation facilitated a rapid response time of 5 s by transferring electrons efficiently to the electrode surface. The Naf/UOx/Fc system produced a linear response over a wide range (500 nM to 600 μM). Hence the sensor could be useful for the direct estimation of UA level in human serum. The system was highly sensitive (1.86 μA μM^{-1}). The low K_m" (14.07 μM) showed the high affinity of UOx towards UA even after immobilisation. The system was stable for about seven weeks. The coefficients of variation for repeatability and reproducibility were found to be only 1.6% and 2.1%, respectively. Furthermore, the Naf/UOx/Fc/GCE showed excellent selectivity towards UA in the presence of interfering agents such as ascorbic acid, glucose and xanthine. The use of the sensing system i.e. a Naf/UOx/Fc biosensor on serum samples proved fruitful with a confidence limit of more than 95% compared to the standard laboratory method.

Acknowledgements

The authors gratefully acknowledge the financial support from the Department of Biotechnology, Government of West Bengal (Sanction No:1695/71 state; dated 16/06/2009) and special thanks to Dr. Trivedi and Roy Clinic for providing serum samples for the analysis. Ms. Ghosh is thankful to the Central Instrument Facility Services, Bose Institute, Kolkata for providing the experimental facilities on CD spectropolarimeter and fluorescence spectrophotometer.

Appendix A. Supplementary data

Supplementary data to this article can be found online at http://dx.doi.org/10.1016/j.bioelechem.2014.11.001.

References

[1] S.J. Kelly, M. Delnomdedied, M.I. Oliverio, L.D. Williams, M.G.P. Saifer, M.R. Shierman, T.M. Cofferman, G.A. Johnson, M.S. Hershfield, Diabetes insipidus in uricase-deficient mice: a model for evaluating therapy with poly(ethylene glycol)-modified uricase, J. Am. Soc. Nephrol. 12 (2001) 1001–1009.
[2] C.A. Burtic, E.R. Ashwood, Tietz Textbook of Clinical Chemistry, 2nd edn. Saunders, Philadelphia, 1994.
[3] Y.M. Marickar, Calcium oxalate stone and gout, Urol. Res. 37 (2009) 345–347.
[4] BioAssay Systems, QuantiChrom™ Uric Acid Assay Kit (DIUA-250) [Internet], http://www.medibena.at/media/BAS/product-sheets/diua.pdf2007 (Accessed January 2010).
[5] The Amplex Red Uric Acid/Uricase Assay Kit, Molecular Probes®, Invitrogen Detection Technology[Internet] http://tools.lifetechnologies.com/content/sfs/manuals/mp22181.pdf2004 (Accessed June 2010).
[6] K. Arora, G. Sumana, V. Saxena, R.K. Gupta, S.K. Gupta, J.V. Yakhmi, M.K. Pandey, S. Chand, B.D. Malhotra, Improved performance of polyaniline-uricase biosensor, Anal. Chim. Acta. 594 (2007) 17–23.
[7] J. Kan, X. Pan, C. Chen, Polyaniline-uricase biosensor prepared with template process, Biosens. Bioelectron. 19 (2004) 1635–1640.
[8] G. Yang, L. Tan, Y. Shi, S. Wang, X. Lu, H. Bai, Y. Yang, Direct determination of uric acid in human serum samples using polypyrrole nanoelectrode ensembles, Bull. Kor. Chem. Soc. 30 (2009) 454–458.
[9] F. Zhang, X. Wang, S. Ai, Z. Sun, Q. Wan, Z. Zhu, Y. Xian, L. Jin, K. Yamamoto, Immobilization of uricase on ZnO nanorods for a reagentless uric acid biosensor, Anal. Chim. Acta. 519 (2004) 155–160.
[10] M.S. Usman Ali, Z.H. Ibupoto, M. Kashif, U. Hashim, M. Willander, A potentiometric indirect uric acid sensor based on ZnO nanoflakes and immobilized uricase, Sensors 12 (2012) 2787–2797.
[11] K. Jindal, M. Tomar, V. Gupta, CuO thin film based uric acid biosensor with enhanced response characteristics, Biosens. Bioelectron. 38 (2012) 11–18.
[12] Y. Li, G. Ran, W.J. Yi, H.Q. Luo, N.B. Li, A glassy carbon electrode modified with graphene and poly(acridine red) for sensing uric acid, Microchim. Acta 178 (2012) 115–121.
[13] M. Hadi, A. Rouhollahi, Simultaneous electrochemical sensing of ascorbic acid, dopamine and uric acid at anodized nanocrystalline graphite-like pyrolytic carbon film electrode, Anal. Chim. Acta 721 (2012) 55–60.
[14] Y. Lv, Z. Zhang, F. Chen, Chemiluminescence biosensor chip based on a microreactor using carrier air flow for determination of uric acid in human serum, Analyst 127 (2002) 1176–1179.
[15] A.R. Vijayakumar, E. Csöregi, A. Heller, L. Gorton, Alcohol biosensors based on coupled oxidase-peroxidase systems, Anal. Chim. Acta. 327 (1996) 223–234.
[16] S. Dong, B. Wang, B. Liu, Amperometric glucose sensor with ferrocene as an electron transfer mediator, Biosens. Bioelectron. 7 (1991) 215–222.
[17] S.R. Chinnadayyala, A. Kakoti, M. Santhosh, P. Goswami, A novel amperometric alcohol biosensor developed in a 3rd generation bioelectrode platform using peroxidase coupled ferrocene activated alcohol oxidase as biorecognition system, Biosens. Bioelectron. 55 (2014) 120–126.
[18] R.S. Herrick, R.M. Jarret, T.P. Curran, D.R. Dragoli, M.B. Flaherty, S.B. Lindyberg, R.A. Slate, L.C. Thornton, Ordered conformations in bis(amino acid) derivatives of 1,1′-ferrocenedicarboxylic acid, Tetrahedron. Lett. 52–89 (1996).
[19] M. Liu, Q. Chen, C. Lai, Y. Zhang, J. Deng, H. Li, S. Yao, A double signal amplification platform for ultrasensitive and simultaneous detection of ascorbic acid, dopamine, uric acid and acetaminophen based on a nano composite of ferrocene thiolate stabilized Fe_3O_4@Au nanoparticles with graphene sheet, Biosens. Bioelectron. 48 (2013) 75–81.
[20] A.E.G. Cass, G. Davis, G.D. Francis, H.A.O. Hill, W.J. Aston, I.J. Higgins, E.V. Plotkin, L.D.L. Scott, A.P.F. Turner, Ferrocene-mediated enzyme electrode for amperometric determination of glucose, Anal. Chem. 56 (1984) 667–671.
[21] S.H. Liu, W.M. Mo, F. Chen, An amperometric enzyme electrode for glucose by immobilizing glucose oxidase and ferrocene in β-cyclodextrin, J. Instrum. Anal. 18 (1999) 42–45.
[22] G.R. Zhang, X.L. Wang, X.W. Shi, T.L. Sun, β-Cyclodextrin–ferrocene inclusion complex modified carbon paste electrode for amperometric determination of ascorbic acid, Talanta 51 (2000) 1019–1025.
[23] S. Wang, D. Du, Differential pulse voltammetry determination of ascorbic acid with ferrocene-l-cysteine self-assembled supramolecular film modified electrode, Sensors Actuators B 97 (2004) 373–378.
[24] J.D. Qiu, H.P. Peng, R.P. Liang, Ferrocene-modified Fe_3O_4@SiO_2 magnetic nanoparticles as building blocks for construction of reagentless enzyme-based biosensors, Electrochem. Commun. 9 (2007) 2734–2738.
[25] A. Senthil Kumar, S. Sornambikai, Selective amperometric sensing of hydrogen peroxide with nafion/copper particulates chemically modified electrode, Indian J. Chem. 48 (2009) 940–945.
[26] L. Yumei, F. Zhiqiang, D. Kejun, T. Yifeng, Study on a pyruvate oxidase biosensor based on β-cyclodextrin with ferrocene as electron-transfer mediator, Anal. Lett. 42 (2009) 312–322.
[27] M. Chen, X. Wei, H. Qian, G. Diao, Fabrication of GNPs/CDSH-Fc/nafion modified electrode for the detection of dopamine in the presence of ascorbic acid, Mater. Sci. Eng. C 31 (2011) 1271–1277.
[28] Y. Zhao, X. Yan, Z. Kang, P. Lin, X. Fang, Y. Lei, S. Ma, Y. Zhang, Highly sensitive uric acid biosensor based on individual zinc oxide micro/nanowires, Microchim. Acta 180 (2013) 759–766.
[29] M. Das, P. Goswami, Direct electrochemistry of alcohol oxidase using multi-walled carbon nanotube as electroactive matrix for biosensor application, Bioelectrochemistry 89 (2013) 19–25.
[30] T. Ghosh, P. Sarkar, Isolation of a novel uric acid degrading microbe Comamonas sp. BT UA and rapid biosensing of uric acid from extracted uricase enzyme, J. Biosci 39 (2014) 805–819.
[31] A.A. Ghoneim, Electrochemical behavior of vanadium in azide electrolyte in comparison with the behavior in halogen ions-containing electrolytes, Open Electrochem. J. 1 (2009) 42–48.
[32] A.J. Bard, L.R. Faulkner, Electrochemical Methods: Fundamentals and Applications, second ed. Wiley, New York, 2001.
[33] The Sadtler Standard Spectra, Standard Infrared Grating Spectra, ©1973 Sadtler Research Laboratories Inc., Subsidiary of Block Engineering Inc., 28121 K.
[34] G. Wang, W. Xing, S. Zhuo, Application of mesoporous carbon to counter electrode for dye-sensitized solar cells, J. Power Sources 194 (2009) 568–573.

[35] M. Liu, L. Wang, Y. Meng, Q. Chen, H. Li, Y. Zhang, S. Yao, (4-Ferrocenylethyne) phenylamine functionalized graphene oxide modified electrode for sensitive nitrite sensing, Electrochim. Acta 116 (2014) 504–511.
[36] M. Liu, J. Deng, Q. Chen, Y. Huang, L. Wanga, Y. Zhao, Y. Zhang, H. Li, S. Yao, Sensitive detection of rutin with novel ferrocene benzyne derivative modified electrodes, Biosens. Bioelectron. 41 (2013) 275–281.
[37] J.S.N. Dutt, M.F. Cardosi, J. Davis, Electrochemical tagging of urate: developing new redox probes, Analyst 128 (2003) 811–813.
[38] M. Liu, L. Wang, J. Deng, Q. Chen, Y. Li, Y. Zhang, H. Li, S. Yao, Highly sensitive and selective dopamine biosensor based on a phenylethynyl ferrocene/graphene nanocomposite modified electrode, Analyst 137 (2012) 4577–4583.
[39] J.G. Velasco, Determination of standard rate constants for electrochemical irreversible processes from linear sweep voltammograms, Electroanalysis 9 (1997) 880–882.
[40] R.S. Staden, R.M. Nejem, J.F. Staden, H.Y. Aboul-Enein, Amperometric biosensor based on diamond paste for the enantioanalysis of L-lysine, Biosens. Bioelectron. 35 (2012) 439–442.

Tanushree Ghosh received her B.Sc degree in Zoology from University of Calcutta in 2006 and M.Sc. degree in Biotechnology from Jadavpur University in 2008. She is now working for her Ph.D. in the Department of Polymer Science and Technology, University of Calcutta. She is working in the area of microbial enzymology, recovery of enzyme and chemical biosensors for applications in biomedical and food technology.

P. Sarkar is a Professor in the Department of Polymer Science and Technology, University of Calcutta, West Bengal. Prof. Sarkar is a Chemical Engineer from Jadavpur University. He received his PhD degree from IIT Kanpur. He has 25 years of research and teaching experience and published number of papers in International journals. His areas of research interest include design and applications of electrochemical sensors, removal of toxic heavy metals from drinking water, and bioremediation.

Anthony P.F. Turner, Editor-in-chief, *Biosensors and Bioelectronics,* was formerly Principal of Cranfield University at Silsoe (UK) and Distinguished Professor of Biotechnology. He joined Linköping University in 2010, to create a new *Centre for Biosensors and Bioelectronics*. He was elected Fellow of the Royal Society of Chemistry (UK) in 1996, Foreign Associate of the National Academy of Engineering (USA) in 2006 and to the Royal Swedish Academy of Engineering in 2013. He gained his PhD in 1980 and was awarded a Higher Doctorate (DSc) by the University of Kent in 2001 and Honorary DSc by the University of Bedfordshire in 2008. He is best known for his contributions to glucose sensors, environmental monitors and synthetic recognition molecules.